The E_8–manifold, singular fibers and handlebody decompositions

ROBION KIRBY
PAUL MELVIN

Abstract The E_8–manifold has several natural framed link descriptions, and we give an efficient method (via "grapes") for showing that they are indeed the same 4–manifold. This leads to explicit handle pictures for the perturbation of singular fibers in an elliptic surface to a collection of fishtails. In the same vein, we show how the degeneration of a regular fiber to a singular fiber in an elliptic surface provides rich examples of Gromov's compactness theorem.

AMS Classification 57N13; 57R65,14J27

Keywords 4–manifolds, handlebodies, elliptic surfaces

0   Introduction

The E_8 –*manifold* is the 4–manifold obtained by plumbing together eight copies of the cotangent disk bundle of the 2–sphere according to the Dynkin diagram for the exceptional Lie group E_8 (Figure 0.1a). As a handlebody, this is given by the framed link shown in Figure 0.1b [10].[†] The boundary of E_8 is the Poincaré homology sphere (see for example [11]).

Alternatively, E_8 may be obtained by taking the p–fold cover of the 4–ball branched over the standard Seifert surface for the (q,r)–torus knot (pushed into the interior of B^4) where (p,q,r) is a cyclic permutation of $(2,3,5)$.

In section 1, the calculus of framed links [10] is used to prove that these four 4–manifolds (E_8 and the three branched covers) are diffeomorphic. This result

---

[†]Sometimes the tangent bundle is used, giving $+2$ framings, but by changing the orientation of the 4–manifold, which negates the linking matrix of the corresponding framed link, and then the orientation of alternate 2–spheres to restore the off diagonal elements in the linking matrix, we get an orientation reversing diffeomorphism between these two descriptions; as a complex manifold, -2 is natural.

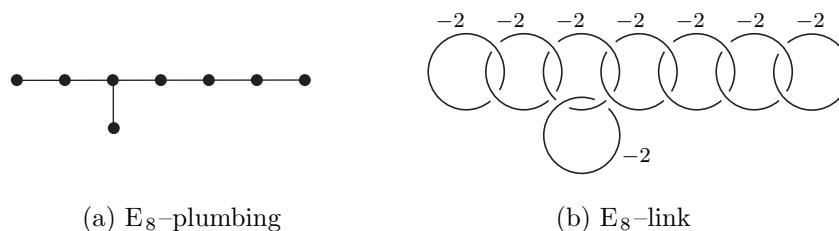(a) E_8–plumbing   (b) E_8–link

Figure 0.1

is not new. Algebraic geometers knew this at least as long ago as Kodaira, and it is a special case of work of Brieskorn [2, 3] which we outline now.

Consider the solution V_ε to $x^2 + y^3 + z^5 = \varepsilon$ in $B^6 \subset \mathbb{C}^3$. This variety is a nonsingular 4–manifold (for small $\varepsilon \neq 0$) which can be described as, for example, the 2–fold branched cover of B^4 along the curve $y^3 + z^5 = \varepsilon$ (well known to be the usual Seifert surface for the $(3, 5)$–torus knot). Similarly V_ε can be viewed as a 3 or 5–fold branched cover.

The variety V_0, equal to V_ε for $\varepsilon = 0$, is a cone on ∂V_ε and has an isolated singularity at the origin. The singularity can be resolved to obtain a nonsingular complex surface, called V_{res} (see [7] for an exposition for topologists of resolving singularities). Brieskorn proved that V_{res} is diffeomorphic to V_ε when the isolated singular point is a *simple* singularity or a *rational double point*, and these are related to the simple Lie algebras [4]. If these 4–manifolds are described using framed links, then the algebraic–geometrical proofs do not immediately give a procedure for passing from one framed link to the other; in particular it is not clear how complicated such a procedure might be. So a method is given in section 1. The steps in Figure 1.7 from the E_8–link to the "bunch of grapes" (Figure 1.3b) are the most interesting.

Section 2 of the paper is concerned with the various singular fibers that can occur in an elliptic surface. These were classified by Kodaira [12] and a description for topologists can be found in [7] or the book of Gompf and Stipsicz [5] (also see section 2). A singular fiber, when perturbed, breaks up into a finite number of the simplest singular fibers; these are called *fishtails* and each consists of an immersed 2–sphere with one double point. Thus a neighborhood of a singular fiber should be diffeomorphic to a neighborhood of several fishtails, and this is known to be diffeomorphic to a thickened regular fiber, $T^2 \times B^2$, with several 2–handles attached to vanishing cycles. Constructing these diffeomorphisms is the subject of Section 2.

This can be looked at from a different perspective. Gromov's compactness theorem [6] for (pseudo)holomorphic curves in (almost) complex surfaces says that

a sequence of curves can only degenerate in the limit by pinching loops in the domain so as to bubble off 2–spheres, and then mapping the result by a holomorphic map (often just a branched covering) onto its image. When showing that fishtails equal a singular fiber, one gets an idea of how a torus fiber degenerates onto the singular fiber (the limiting curve in Gromov's sense). Section 3 contains a discussion of this degeneration for each of Kodaira's singular fibers.

1   Handlebody descriptions of the E_8–manifold

The E_8–manifold can be constructed by adding 2–handles to the framed link in $S^3 = \partial B^4$ drawn in Figure 0.1b, and again in Figures 1.1a and 1.1b using successively abbreviated notation which we now explain.
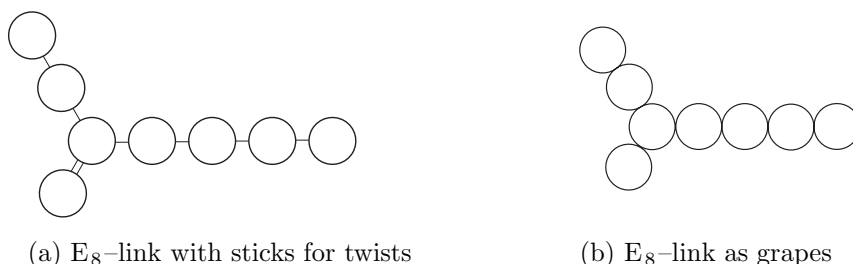

(a) E_8–link with sticks for twists   (b) E_8–link as grapes

Figure 1.1

Grapes

In Figure 1.1a the "stick" notation $\rightthreetimes$ denotes a full left twist $\lessgtr$ between the vertical strands, while $\leftthreetimes$ denotes a full right twist $\gtrless$. The framings (when not labelled) should be assumed to be -2. This convention, which will be used throughout the paper, is convenient because handle slides typically occur for 2–handles A and B with intersection number ± 1 (where we identify a 2–handle with its associated homology class), so sliding A over B yields the class $A \pm B$ with self-intersection $(A \pm B)^2 = A^2 \pm 2A \cdot B + B^2 = -2 + 2 - 2 = -2$.

In Figure 1.1b the circles are all required to lie in the hexagonal packing of the plane. The convention is that a tangency between a pair of circles represents a full twist between them, and that this twist is right-handed if and only if the line joining their centers has positive slope. (In particular the drawings in Figure 1.1 represent identical link diagrams.) Framings are -2 as in our standing convention. Any configuration of hexagonally packed circles representing a framed link (and thus a 4–manifold) by these conventions will be refered to as

"grapes"; each individual circle will be called a grape. It will be seen in what follows that the framed links that arise in studying elliptic surfaces and related 4–manifolds can often be represented (after suitable handle-slides) by grapes; this observation will streamline many of our constructions.

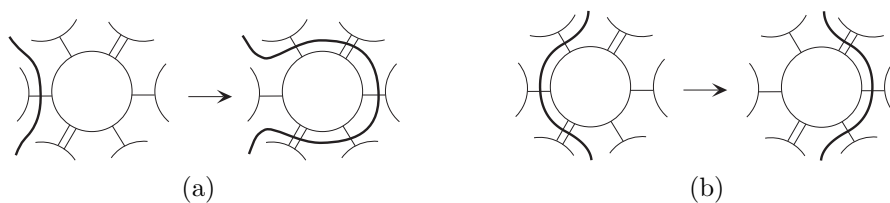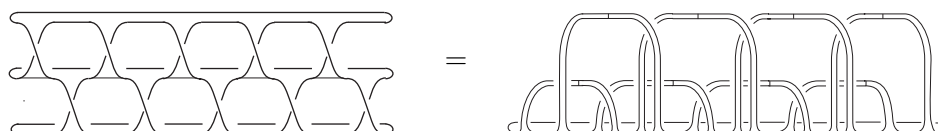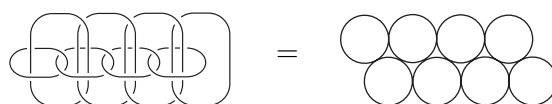Typical handleslides over a grape are illustrated in Figure 1.2, using the stick notation.

(a)   (b)

Figure 1.2: Handleslides over a grape

Branched covers

The 4–manifold C_2 which is the 2–fold branched cover of B^4 along a minimal genus Seifert surface $F_{3,5}$ for the $(3,5)$–torus knot in S^3, pushed into the interior of B^4, is described in the next figures.
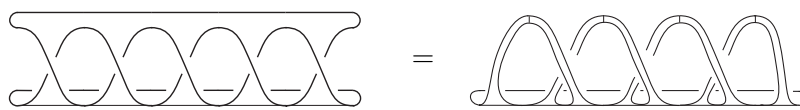

(a) Seifert surface $F_{3,5}$

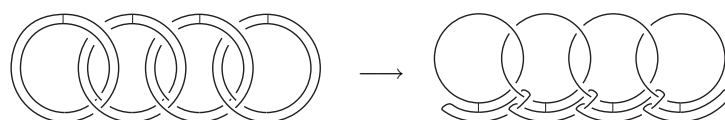(b) Branched cover C_2 as a bunch of grapes

Figure 1.3

Since torus knots are fibered, all Seifert surfaces of minimal genus are isotopic, so the surface in Figure 1.3a will do. Note that the Seifert surface in the first drawing consists of three stacked disks with ten vertical half twisted bands joining them; the front four (large) 1–handles in the second drawing come from the top disk and the upper five half-twisted bands, the back four (small) 1–handles come from the middle disk and lower five half twisted bands, and the 0–handle is the bottom disk.

By the algorithm in [1] for drawing framed link descriptions of branched covers of Seifert surfaces, a half circle should be drawn in each 1–handle, and then these eight half circles should be folded down to get the link shown in Figure 1.3b. The framing on each component is twice the twist in corresponding 1–handle (which is -1), so is -2 and not drawn by convention. Now folding the four smaller components over the top of the larger ones gives the bunch of eight grapes shown in the second drawing.

In a similar way, we draw in Figure 1.4 the Seifert surface $F_{2,5}$ for the $(2,5)$–torus knot, followed by its 3–fold branched cover C_3. In the algorithm (in [1]) *two* half circles are drawn in each of the four 1–handles, and then one set of four is folded down followed by the other set. This produces the first drawing in Figure 1.4b. The second drawing is obtained from the first by sliding the outer 2–handle over the inner 2–handle for each of the four pairs of 2–handles.[†] This link clearly coincides with the bunch of grapes in Figure 1.3b, showing that C_3 is diffeomorphic to C_2.
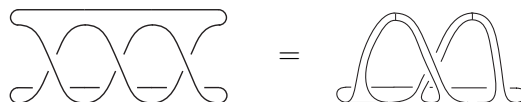

(a) Seifert surface $F_{2,5}$
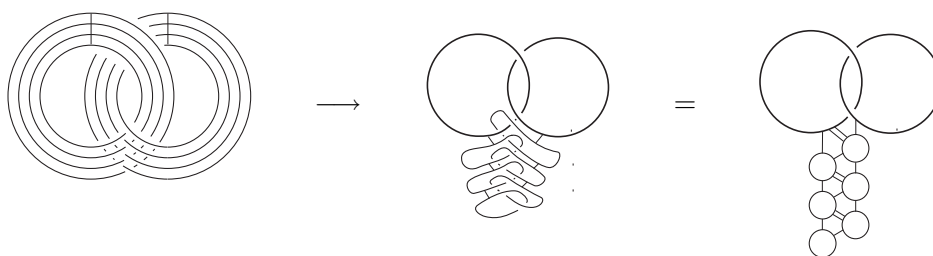

(b) Branched cover C_3 (same bunch of grapes)

Figure 1.4

Finally, Figure 1.5 shows the Seifert surface $F_{2,3}$ for the $(2,3)$–torus knot and its 5–fold branched cover C_5 (where)∦(denotes a full left twist in the vertical strands). To pass from the first drawing in 1.5b to the second we perform six handleslides, sliding each circle over its parallel neighbor, starting with the outermost circles and working inward. Rotating the last drawing by a quarter turn yields the same bunch of grapes,[†] showing that C_5 is diffeomorphic to C_2.

[†]In fact there are two algorithms in [1] for drawing the cover (see Figures 5 and 6 in [1]). The first (which is more natural but often harder to visualize) yields the grapes directly. The second is derived from the first by sliding handles — the reverse of the slides above in the present case.
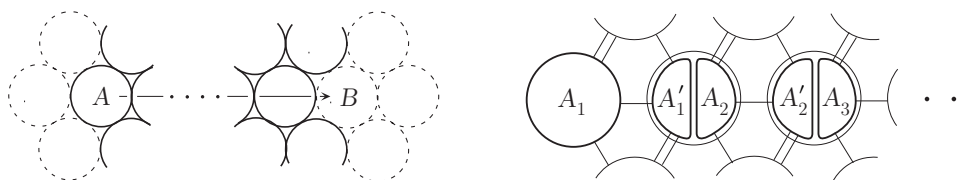
(a) Seifert surface $F_{2,3}$

(b) Branched cover C_5 (same bunch of grapes)

Figure 1.5

Equivalence of handlebody decompositions

To show that these covers are diffeomorphic to E_8, we introduce a move on an arbitrary cluster of grapes (configuration of hexagonally packed circles), called a *slip* [13], which amounts to a sequence of handle slides and isotopies: Suppose that such a cluster contains a grape (labelled A in Figure 1.6a) which is the first of a straight string of grapes, in *any of the six possible directions*. If there are no grapes in the dotted positions shown in Figure 1.5a, then grape A can be moved by a *slip* to the other end of the the string, that is to the position of the dotted grape B in the figure. (Note that this slip can be reversed.)

(a) a slip

(b) the anatomy of a slip

Figure 1.6

The handle slides and isotopies which produce the slip are indicated in Figure 1.6b: $A = A_1 \rightsquigarrow A'_1 \to A_2 \rightsquigarrow A'_2 \to A_3 \rightsquigarrow \cdots \to A_n \rightsquigarrow B$. Here $A_i \rightsquigarrow A'_i$ is the obvious isotopy (folding under when moving horizontally, folding over

when moving along the line inclined at $-\pi/3$ radians, and moving in the plane of the paper by a regular isotopy when moving along the line inclined at $\pi/3$ radians) as the reader can easily check, and A_{i+1} is obtained by sliding A'_i over its encircling grape (cf Figure 1.2b).

Finally observe that the sequence of seven slips shown in Figure 1.7 takes the grapes defining E_8 (Figure 1.1b) to the grapes for the branched cover C_2 (Figure 1.3b).
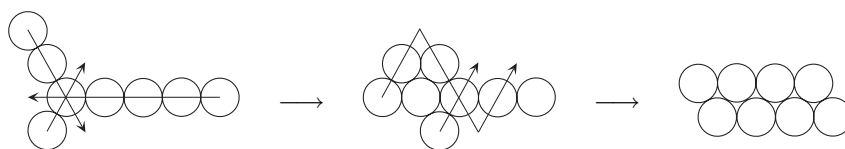

Figure 1.7: slippin' an' a slidin'

Note that in the middle picture, the single slip must be performed before the last leg of the triple slip.

2   Singular fibers in elliptic surfaces

The E_8–manifold occurs naturally as a neighborhood of (most of) a singular fiber in an elliptic surface, and so the discussion in the last section suggests a general study of such neighborhoods. We begin with a brief introduction to the topology of elliptic surfaces and their singular fibers; much fuller accounts for topologists appear in [5] and [7].

An *elliptic surface* is a compact complex surface E equipped with a holomorphic map $\pi\colon E \to B$ onto a complex curve B such that the each *regular fiber* (preimage of a regular value of π) is a non-singular elliptic curve — topologically a torus — in E. Thus E is a T^2–bundle over B away from the (finitely many) critical values of π. The fibers over these critical values are called the *singular fibers* of the surface.

Each singular fiber C in E is a union of irreducible curves C_i, the *components* of the fiber. Topologically the components are closed surfaces, possibly with self-intersection or higher order singularities (for example a "cusp"), and distinct components can intersect, either transversely or to higher order. Furthermore, each component has a positive integer *multiplicity* m_i, where $\sum m_i C_i$ represents the homology class of a regular fiber. The multiplicity of C is then defined to be the greatest common divisor of the multiplicities of its components. We

shall limit our discussion to *simple* singular fibers, that is, fibers of multiplicity one.[†] We also assume that E is *minimal*, that is, not a blow-up of another elliptic surface, or topologically not a connected sum of an elliptic suface with $\overline{\mathbb{C}P^2}$. This precludes any *exceptional* components (non-singular rational curves of -1 self-intersection) in singular fibers.

The singular fibers in minimal elliptic surfaces were classified by Kodaira [12], and the simple ones fall into eight classes: two infinite families I_n and I_n^* (where n is a non-negative integer, positive in the first case since I_0 represents a regular fiber), three additional types II–IV and their "duals" II*–IV* (explained below). In all cases the components are rational curves — topologically 2–spheres — and so the singular fiber can be depicted by a *graph* of intersecting arcs representing these components.

Fibers of type I–IV (Table 1)

The two simplest singular fibers are the *fishtails* (type I_1) and the *cusps* (type II). A fishtail consists of a single component, an immersed 2–sphere with one positive double point, and is represented by a self-intersecting arc $\bowtie$. A cusp is a 2–sphere with one singular point which is locally a cone on a right handed trefoil knot; this is denoted by a cusped arc $\prec$.

The components in all other singular fibers (including those of $*$–type) are smoothly embedded 2–spheres with self-intersection -2. In particular, a singular fiber of type III consists of two such 2–spheres which are tangent to first order at one point, denoted by a pair of tangent arcs $\times$, and one of type IV consists of three such 2–spheres intersecting transversely in one triple point, denoted $\asterisk$. Singular fibers of type I_n for $n > 1$, called *necklace fibers*, consist of n such 2–spheres arranged in a cycle, each intersecting the one before it and the one after it (which coincide if $n = 2$). For example $I_2 = \;\lozenge$ and $I_5 = \;\star$. These graphs are reproduced in the first column of Table 1 below; note that all components have multiplicity one in these types of fibers.

The second column in the table gives natural framed link descriptions for regular neighborhoods of these fibers, following [7]. A neighborhood of a fishtail is clearly a self-plumbing of the cotangent disk bundle τ^* of the 2–sphere, of euler class -2 (the homology class represented by the fishtail must have self-intersection zero, so the euler class is -2 to balance the two positive points of intersection arising from the double point) and this can be constructed as a 0–handle with a round 1–handle ($=$ 1–handle plus a 2–handle) attached as

---

[†]All other fibers are either multiples of singular fibers or multiples of regular fibers, and the latter have uninteresting neighborhoods, namely $T^2 \times B^2$.

shown. Similarly a neighborhood of an n–component necklace fiber is a circular plumbing of n copies of τ^*, or equivalently surgery on a chain of circles in $S^1 \times B^3$ ($= 0$–handle plus a 1–handle). The cusp neighborhood is obtained by attaching a single 2–handle along the zero framed right-handed trefoil. Fibers of type II and III are gotten by attaching handles to the $(2,4)$ and $(3,3)$–torus links, respectively, with -2 framings on all components. (In section 3 we will give explicit models for these neighborhoods in which the projection of the elliptic surface is evident.)
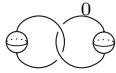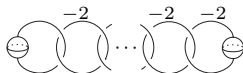
type	graph	framed link	monodromy
I_1			V
$\mathrm{I}_n \; (n \geq 2)$			V^n
II			UV
III			UVU
IV			$(UV)^2$

Table 1: Singular fibers of type I–IV

The final column in the table gives the *monodromy* of the torus bundle around each singular fiber with respect to a suitably chosen basis for the first homology of a regular fiber,[†] given in terms of the generators

$$U = \begin{pmatrix} 1 & 0 \\ -1 & 1 \end{pmatrix} \qquad \text{and} \qquad V = \begin{pmatrix} 1 & 1 \\ 0 & 1 \end{pmatrix}$$

[†]More precisely, if we pick a base point b_0 in B and a basis for the first homology of the fiber over b_0, choose paths connecting b_0 to each critical value p_i of π, and choose small loops γ_i around each p_i, then we get a well defined 2×2–matrix for each singular fiber, representing the monodromy of the torus bundle over the associated γ_i.

of $SL(2, \mathbb{Z})$. Note that $(UV)^6 = I = (UVU)^4$ (since $UVU = VUV$). Also note that if the chosen basis is viewed as a *longitude* and *meridian* of the regular fiber (in that order) then U corresponds to meridianal Dehn twist, and V to a longitudinal one.

The fishtail neighborhood can also be obtained from a thickened regular fiber $N = T^2 \times B^2$ by attaching a 2–handle with framing -1 to an essential embedded circle C (or *vanishing cycle*) lying in a torus fiber in $\partial N = T^2 \times S^1$ (see for example [9]). This changes the trivial monodromy of ∂N by a Dehn twist about C, giving V for the monodromy of the fishtail if C is the longitude in the torus. Figure 2.1a shows the standard handlebody decomposition of N with two 1–handles and a 0–framed "toral" 2–handle (where for convenience we identify the horizontal and vertical directions with the meridian and longitude on the torus fiber), and Figure 2.1b shows the result after attaching the last 2–handle along a vertical (longitudinal) vanishing cycle. This handlebody will be denoted by N_V, and simplifies to the one in the table by cancelling the vertical 1 and 2–handles.

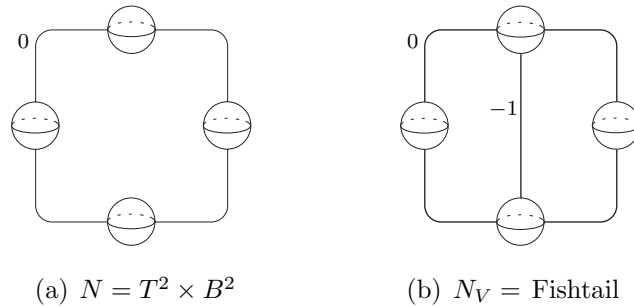(a) $N = T^2 \times B^2$ (b) $N_V = $ Fishtail

Figure 2.1

Now it is well known that any simple singular fiber in an elliptic surface breaks up into finitely many fishtails under a generic perturbation of the projection near the fiber. To show this explicitly for the fibers of type I–IV (the argument for the other types will be given later) observe that the factorization of the monodromy given in Table 1 suggests a pattern of vanishing cycles. For the necklace fiber I_n with monodromy V^n one expects n longitudes. For the remaining types with monodromies $UV \cdots$ the vanishing cycles should alternate between meridians and longitudes.

More precisely, for any word W in U and V, consider the handlebody N_W obtained from N by attaching a sequence of 2–handles along -1–framed meridians (for each U in W) and longitudes (for each V) in successive torus fibers in ∂N. Then we have the following result (cf Theorem 1.25 in [7]).

Theorem 1 *A regular neighborhood of a singular fiber of type* I_n, II, III *or* IV *is diffeomorphic to* N_{V^n}, N_{UV}, N_{UVU} *or* $N_{(UV)^2}$, *respectively.*

Before giving the proof, we describe a general procedure for simplifying N_W, illustrated with the word $W = (UV)^3 V$ (which arises as the monodromy of a fiber of type I_1^* below). The associated handlebody is shown in Figure 2.2a. Sliding each vanishing cycle over its parallel neighbor, working from the bottom up, produces a bunch of grapes (all with framings -2 as usual) hanging from the top horizontal and vertical cycles (Figure 2.2b) — the same process was used to identify the branched covers C_2 and C_5 in the last section (Figure 1.5b). Now cancelling the 2–handles attached to these last two cycles with the 1–handles gives the handlebody R_W in Figure 2.2c.[†] This process will be called the *standard reduction* of the handlebody N_W to the *reduced form* R_W.

(a) The handlebody $N_{(UV)^3V}$ (b) Slide to grapes

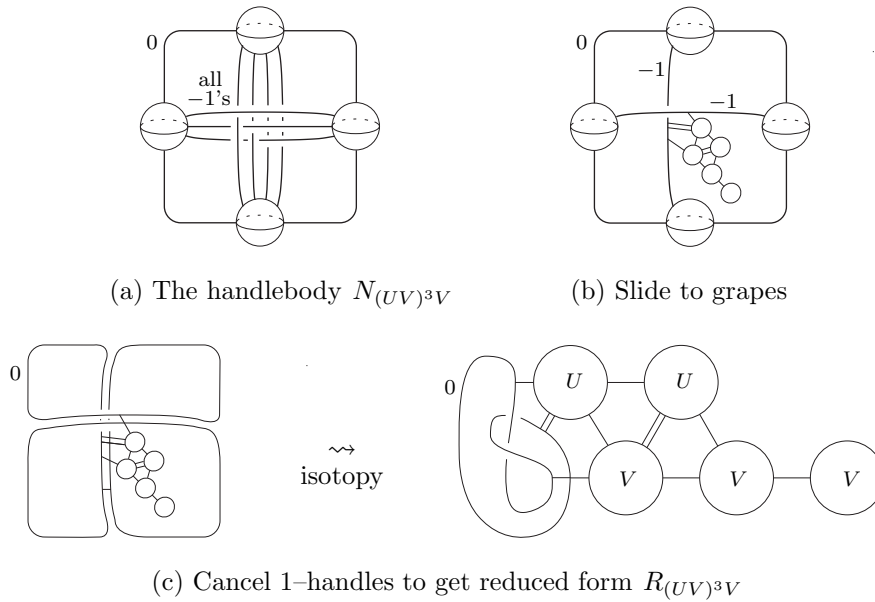(c) Cancel 1–handles to get reduced form $R_{(UV)^3V}$

Figure 2.2: Standard reduction

Observe that the first step of the reduction of N_W (producing the grapes) can be carried out in general, but that the cancellation of *both* 1–handles requires at least one U and one V in W (and the final picture will look slightly different if W does not start with UV). In particular for $W = V^n$ the reduced form R_{V^n}

[†]Note that if one labels the upper row of grapes with U and the lower row with V, as shown, then reading from left to right yields the truncation of W obtained by deleting the initial UV.

is obtained by cancelling the vertical 1–handle with the last vanishing cycle, as shown in Figure 2.3.

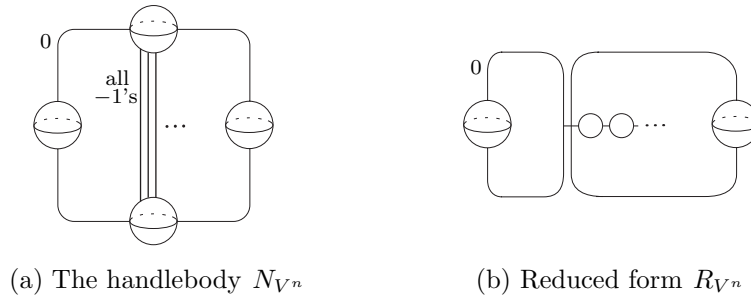(a) The handlebody N_{V^n} (b) Reduced form R_{V^n}

Figure 2.3

We now return to the proof of the theorem. For the necklace fiber I_n, the obvious handleslides of the right-hand loop of the toral 2–handle in R_{V^n} (Figure 2.3b) over the grapes yields the picture for the neighborhood of I_n given in Table 1. For the cusp, the reduced form R_{UV} (shown in Figure 2.4a) is exactly the 0–framed trefoil. For fibers of type III and IV, handleslides of the toral 2–handle in R_{UVU} and $R_{(UV)^2}$ are indicated in Figure 2.4, and an isotopy in each case yields the corresponding picture in the table.
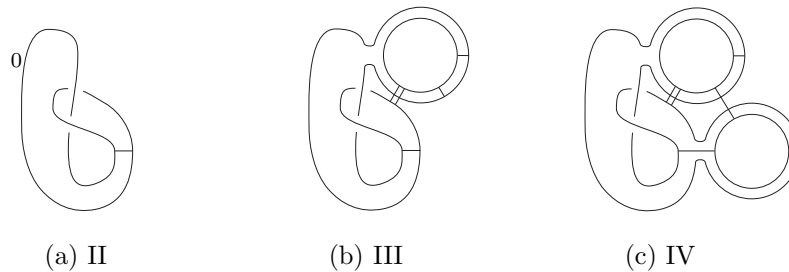

(a) II (b) III (c) IV

Figure 2.4

This completes the proof of Theorem 1. □

Fibers of type I*–IV* (Table 1*)

For the singular fibers of ∗–type, any pair of components intersect transversely in at most one point and there are no "cycles" of components. Thus it is customary to represent these fibers by the *dual tree* with a vertex for each component C_i and an edge joining any two vertices whose associated components intersect. The multiplicities m_i of the components, which are often greater than one, are recorded as weights on the vertices of the tree. Note that the m_i are uniquely

determined by the equations $\sum_i m_i C_i \cdot C_j = 0$ since $\sum_i m_i C_i$ is homologous to a regular fiber which is disjoint from C_j; this translates into the condition that the weight of each vertex is half the sum of the weights of its neighboring vertices.

Regular neighborhoods of these fibers are the associated plumbings of the cotangent disk bundle of S^2 (see section 3 for explicit models which explain why these plumbings appear) and can all (with the exception of I_0^*) be represented by grapes as in section 1, in fact in a variety of ways. We choose one, and record it in Table 1* along with the associated weighted tree and monodromy.

type	weighted tree	grapes	monodromy
I_0^*			$(UV)^3 = -I$
I_n^* $(n > 0)$			$(UV)^3 V^n = -V^n$
II*			$(UV)^5 = (UV)^{-1}$
III*			$(UV)^4 U = (UVU)^{-1}$
IV*			$(UV)^4 = (UVUV)^{-1}$

Table 1*: Singular fibers of type I*–IV*

The reader should note the inverse relation between the monodromies of each fiber of type II–IV and its starred counterpart, which provides one explanation for their common label. This implies that neighborhoods of dual fibers (ie, II and II*, III and III*, or IV and IV*) can be identified along their boundaries to form a (closed) elliptic surface. Indeed one obtains in this way various non-generic projections of the rational elliptic surface $E(1)$, diffeomorphic to $\mathbb{C}P^2 \# 9\overline{\mathbb{C}P^2}$, whose generic projection has twelve fishtails (see eg [7, section 1]).

We now state the analogue of Theorem 1.

Theorem 1[*] *A regular neighborhood of a singular fiber of type* I_n^*, II*, III* *or* IV* *is diffeomorphic to* $N_{(UV)^3V^n}$, $N_{(UV)^5}$, $N_{(UV)^4U}$ *or* $N_{(UV)^4}$, *respectively.*

Proof Proceeding as in the proof of Theorem 1, consider the handleslides of the toral 2–handle over the grapes in the reduced forms, as shown in Figure 2.5.
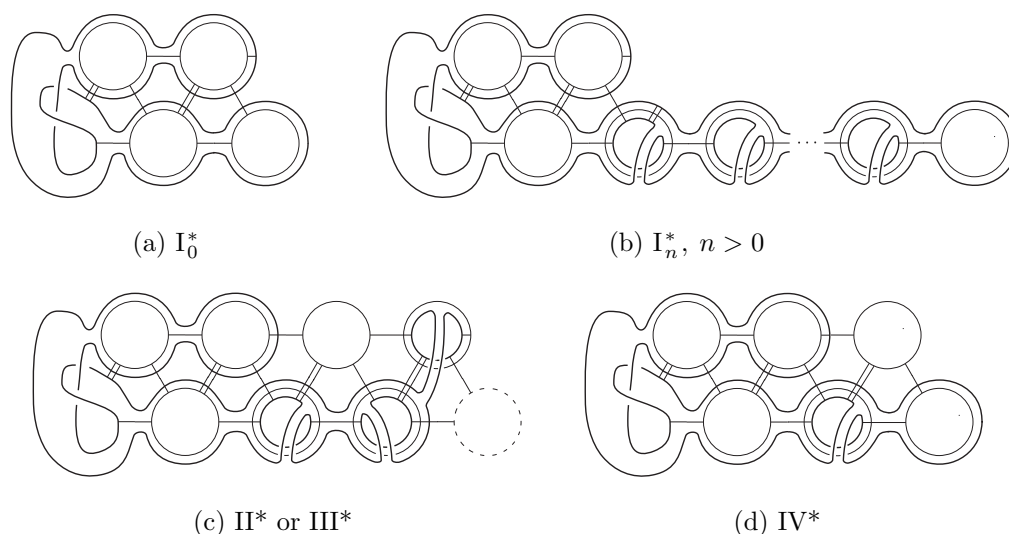

(a) I_0^*

(b) I_n^*, $n > 0$

(c) II* or III*

(d) IV*

Figure 2.5

After an isotopy, the toral 2–handle appears as in Figure 2.6, labelled with a T; note that its framing is now -2. With the exception of I_0^*, the grapes are written in the usual hexagonally packed notation.

We should remark that one is guided in discovering the slides in Figure 2.5 by the multiplicities of the components of the singular fibers, which determine the number of times the toral handle must slide over each grape to achieve the simple pattern in Figure 2.6. However, one must still be very careful in choosing where to perform the slide in order to avoid knotting and linking.

The argument is now completed by a sequence of slips. For singular fibers of type I* (Figure 2.6a,b) a single slip of grape A over grape B does the job, recovering the handlebodies given in Table 1*. For types II*–IV*, the sequence of slips shown in Figure 2.7 will give the clusters of grapes given in the table. Note that if T links only one of the grapes, then that grape can be slipped over others while carrying T along for the ride.

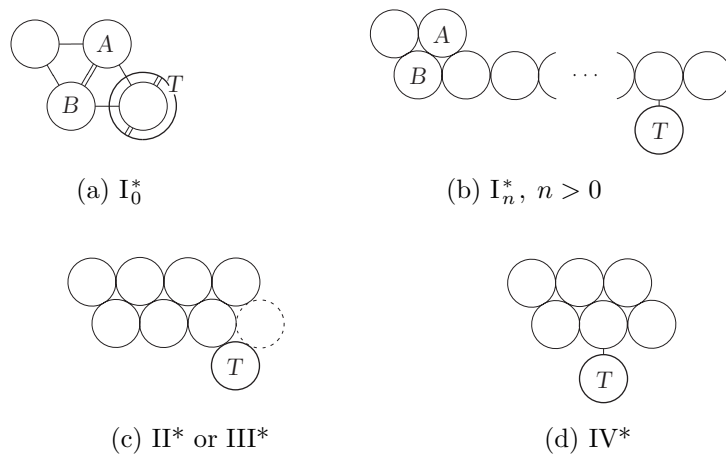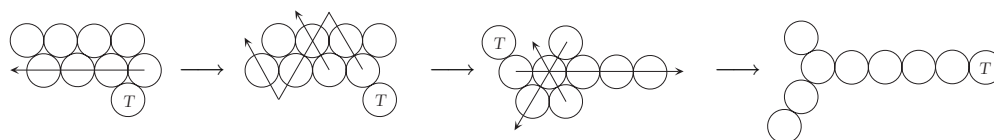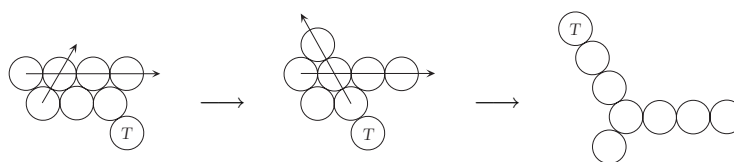This completes the proof of Theorem 1*.   □

(a) I_0^*

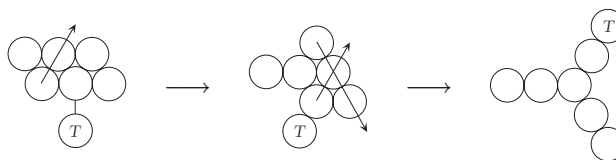(b) I_n^*, $n > 0$

(c) II* or III*

(d) IV*

Figure 2.6

(a) Slips for II*

(b) Slips for III*

(c) Slips for IV*

Figure 2.7

3 Gromov's compactness theorem

In this section we state Gromov's compactness theorem for pseudo-holomorphic curves [6], and then show how this theorem is richly illustrated by the conver-

gence of a sequence of regular fibers to a singular fiber in an elliptic surface.

Pseudo-holomorphic curves and cusp curves

A *pseudo-holomorphic curve* in an almost complex manifold V is a smooth map $f\colon S \to V$ of a Riemann surface S into V whose differential at each point is complex linear. This means $df \circ j = J \circ df$, where J is the almost complex structure on V (a bundle map on τ_V with $J^2 = -I$ on each fiber) and j is the (almost) complex structure on S.[†] We also write

$$f\colon (S, j) \to V$$

to highlight the complex structure on S, which may vary; the almost complex structure on V is assumed fixed.

Cusp curves are generalizations of pseudo-holomorphic curves in which one allows the domain to be a *singular* Riemann surface $\bar{S}$, obtained by crushing each component C_i of a smoothly embedded 1–manifold C in S to a point p_i. Each singular point p_i is to be viewed as a *transverse* double point of $\bar{S}$ with distinct complex structures on the two intersecting sheets. To make this precise, consider (following Hummel [8]) the *smooth* surface $\hat{S}$ obtained from $S - C$ by one-point compactifying each end separately, and let $\alpha\colon \hat{S} \to \overline{S}$ be the natural projection. A complex structure $\bar{j}$ on $\bar{S}$ is by definition a complex structure $\hat{j}$ on $\hat{S}$. The pair $(\bar{S}, \bar{j})$ is then called a *singular Riemann surface*, and a map

$$\bar{f}\colon (\bar{S}, \bar{j}) \to V$$

is called a *cusp curve* if $\hat{f} = \bar{f} \circ \alpha\colon (\hat{S}, \hat{j}) \to V$ is pseudo-holomorphic. This setup is illustrated in Figure 3.1. Note that because of dimension limitations a tangency has been drawn at the singular points p_i, but these should be thought of as transverse intersections; indeed $\bar{f}$ can map these to transverse double points as for example occur in the core of a plumbing. Examples of cusp curves are given below.

We also need the notion of a *deformation* of S onto $\bar{S}$, which by definition is any continuous map $d\colon S \to \bar{S}$ which sends each C_i to p_i, and $S - \cup C_i$ diffeomorphically onto $\bar{S} - \cup p_i$.

Gromov's compactness theorem

Let $f_k\colon (S, j_k) \to V$ (for $k = 1, 2, \dots$) be a sequence of pseudo-holomorphic curves. Suppose that V has a Hermitian metric and that there is a uniform

---

[†]The complex structure on S is determined by j, since almost complex structures are integrable in complex dimension 1.
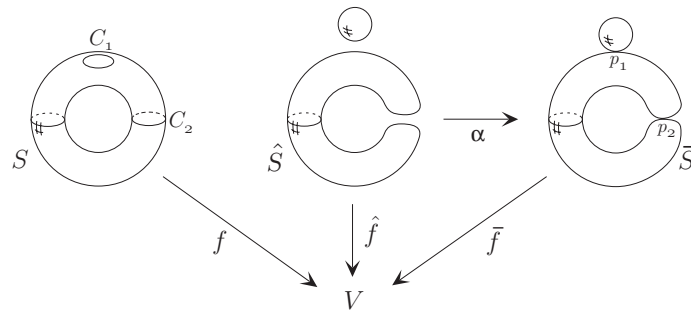
Figure 3.1

bound for the areas of the images $f_k(S)$. (The last condition is automatic if V is symplectic and all $f_k(S)$ belong to the same homology class [8, page 82].)

Then Gromov's compactness theorem states that some subsequence of f_k weakly converges to a cusp curve $\bar{f}: (\bar{S}, \bar{j}) \to V$, where *weakly converges* means (for k now indexing the subsequence):

(1) there exist deformations $d_k: S \to \bar{S}$ such that the complex structures $(d_k^{-1})^* j_k$ on $\bar{S}$ minus the singular points converge in the C^∞ topology to $\bar{j}$ away from the singular points;

(2) $f_k \circ d_k^{-1}$ converges in C^∞ and uniformly to $\bar{f}$ away from the singular points;

(3) the areas of the $f_k(S)$ converge to the "area" of $\bar{f}(\bar{S})$ ($=$ area of $\hat{f}(\hat{S})$).

Remarks

- If the complex structures j_k are all identical, then the curves C_i above must be null-homotopic and thus bound disks in S (see section 3 in Chapter V of [8]). The standard example is given by the sequence of pseudo-holomorphic curves $f_k: S^2 \to S^2 \times S^2$ defined by $f_k(z) = (z, 1/(k^2 z))$ which converges to the two curves $S^2 \times 0 \cup 0 \times S^2$. This process is called *bubbling off* because of the appearance of the extra 2–sphere $0 \times S^2$. A sequence of circles that pinch to $(0,0)$ is $C_k = \{z : |z| = 1/k\}$.

- When the complex structures j_k are not identical, then we may assume that they determine hyperbolic structures (taking out three points if $S = S^2$ or one point if $S = T^2$) and then $\bar{S}$ is the limit in the sense of degeneration of hyperbolic structures. This will be the case with the fishtail singularities below.

- That the deformations d_k are necessary can be seen by considering the case $S = V = T^2$ with $f_k \colon T^2 \to T^2$ equal to the kth power of a Dehn twist around a meridian. This sequence weakly converges to the identity if we take $d_k = f_k$, but has no weakly convergent subsequence if the d_k are independent of k.

Examples

Our collection of examples arise from the fact that a sequence of regular fibers in an elliptic surface which converge to a singular fiber form an illustration of Gromov's Theorem.

To study this convergence, it is useful to have explicit models for the projection of the elliptic surface near the singular fibers. In particular, neighborhoods of the singular fibers with finite monodromy — namely those of type I_0^*, II, II*, III, III*, IV and IV* — can be obtained by taking the quotient of $T^2 \times B^2$ by a finite group action followed by resolving singular points and, perhaps, blowing down. Since the finite group action preserves a natural complex structure on T^2, it follows that all regular fibers in these neighborhoods have the same complex structure, so the circles that are pinched in the compactness theorem are all null-homotopic. Thus in these cases, only bubbling off occurs. In the other cases — namely I_n and I_n^* for $b \geq 1$ — the monodromy is infinite, and the complex structure differs from fiber to fiber. Thus pinching of essential circles is allowed, and in fact necessary in these cases.

We now discuss each of the different types of singular fibers.

Type I A neighborhood of the fishtail I_1 is obtained from $T^2 \times B^2$ by adding a 2–handle to a vanishing cycle, for example a meridian of the torus. This indicates that there is no bubbling off, and that, after removing a point from the torus to make it hyperbolic, a shortest geodesic representing the meridian shrinks (neck stretching) to a point in the limit. Near this point, using local coordinates (z, w), the projection to S^2 is given by the product zw and the preimage of zero is the two axes. Nearby the preimage is $zw = \epsilon$ which is an annulus. Note that the point that was removed to get a hyperbolic structure turns out to be a removable singularity, that is, the pseudo-holomorphic map on the punctured torus extends to the torus, and this is true in the limit.

For I_n with $n > 1$, there are n parallel vanishing cycles, so we remove n points from T^2, interspersed so that the n meridians are not homotopic. Then these meridians shrink as in the case of I_1, and we get a necklace of n spheres in the limit. Note that these spheres have multiplicity one, so their sum is homologous

to a regular fiber and hence has square zero. This implies that each 2–sphere has self-intersection -2.

Type I* First consider the case I_0^*. The monodromy is of finite order, namely two, so we begin with a simple $\mathbb{Z}_2$–action. View the torus as the unit square with opposite sides identified, or equivalently the quotient of $\mathbb{C}$ by the lattice $\langle 1, i \rangle$ (with the induced complex structure). Let σ_2 be the involution on T^2 which rotates the square (or $\mathbb{C}$) by π (Figure 3.2a). Clearly the quotient $X = T^2/\sigma_2$ is a 2–sphere, and the projection $T^2 \to X$ is a 2–fold cover branched over four points corresponding to the center a and vertex b of the square, and the two pairs c and c' of midpoints on opposite edges.
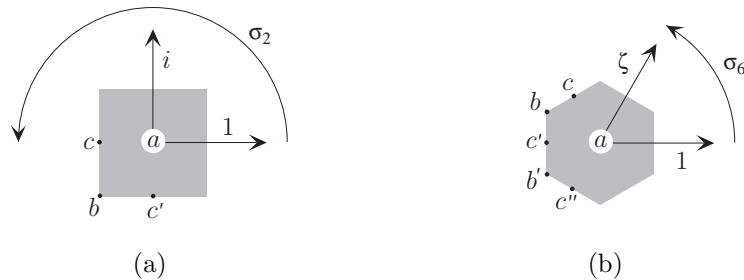

Figure 3.2: Automorphisms of T^2

Set $E = T^2 \times B^2 / \sigma_2 \times \tau_2$ and $D = B^2/\tau_2 \cong B^2$, where τ_r is the rotation of B^2 by $2\pi/r$. Then the natural projection $E \to D$ has a singular fiber over $0 \in D$, namely X, and is a T^2–bundle over $D - 0$ with monodromy $-I$. The space E is a 4–manifold except at the four branch points on X which are locally cones on $\mathbb{R}P^3$. These singular points can be resolved by removing the open cones on $\mathbb{R}P^3$ and gluing in cotangent disk bundles of S^2 with cores A, B, C and D. This gives a neighborhood $N(I_0^*)$ of the singular fiber I_0^*, as shown in Figure 3.3. Note that $2X + A + B + C + D$ is homologous to a regular fiber and hence has square zero, which implies that $X \cdot X = -2$. The second picture is the standard (dual) plumbing diagram, where the vertex weights are the multiplicities.

Now the picture for Gromov's compactness theorem is clear (Figure 3.4). The torus bubbles off four 2–spheres at the branch points (labelled $a-d$) and then double covers X while the four bubbles hit $A-D$ with multiplicity one. (Note that the complex structures on all the torus fibers are the same since the group action is holomorphic, and so we expect to see only bubbling off.) The picture is drawn so that the branched covering transformation σ_2 corresponds to a
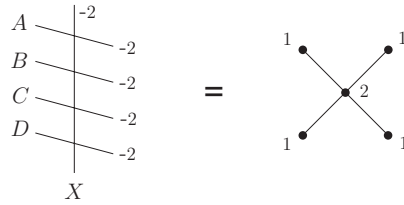
Figure 3.3: $N(\mathrm{I}_0^*)$

π–rotation about the vertical axis through the branched points. As above, tangencies in the picture of I_0^* correspond to transverse double points in $N(\mathrm{I}_0^*)$.
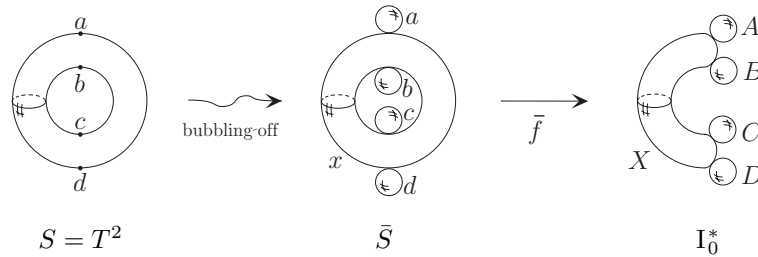

Figure 3.4: Degeneration to I_0^*

For I_n^* with $n > 0$, as in the cases I_n above, the monodromy is of infinite order. Nonetheless, this case is related to I_0^* in that we perform the same construction and in addition shrink n pairs of meridional circles, each pair having the same image under the double covering map. We get $\bar{S}$ as drawn in Figure 3.5, and it is mapped onto the singular fiber in the obvious way: each sphere labelled with a lower case letter maps one-to-one onto the sphere with the corresponding upper case letter and subscript, with the exception of x_1 and x_n which map by 2–fold covers to X_1 and X_n.
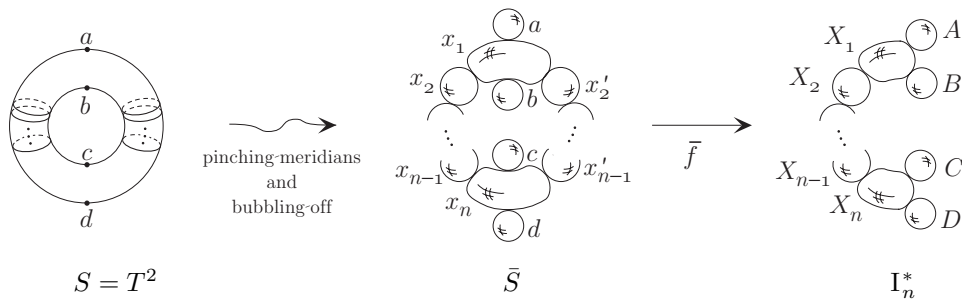

Figure 3.5: Degeneration to I_n^*

Type II View the torus as the hexagon with opposite sides identified, or equivalently the quotient $\mathbb{C}/\langle 1, \zeta \rangle$ where $\zeta = \exp(2\pi i/6)$. Let σ_6 be the automorphism of T^2 of order 6 which rotates the hexagon (or $\mathbb{C}$) by $2\pi/6$. The generic orbit of this action has six points. However, the center a of the hexagon is a fixed point with stabilizer $\mathbb{Z}_6$, the vertices form an orbit with two points b, b' and stabilizer $\mathbb{Z}_3$, and the midpoints of the sides form an orbit with three points c, c', c'' and stabilizer $\mathbb{Z}_2$ (see Figure 3.2b). The quotient $X = T^2/\sigma_6$ is again a 2–sphere, and the projection $T^2 \to X$ is a 6–fold (irregular) cover branched over three points with branching indices 6, 3, and 2.

Set $E = T^2 \times B^2/\sigma_6 \times \tau_6$ and $D = B^2/\tau_6 \cong B^2$. The projection $E \to D$ has the singular 2–sphere X over $0 \in D$, and is a bundle over $D - 0$ with monodromy $\begin{pmatrix} 1 & 1 \\ -1 & 0 \end{pmatrix}$ $(= UV$ for U and V as in section 2). As before, E is a manifold except at the three branch points on X which are locally cones on $L(6, 1)$, $L(3, 1)$, and $L(2, 1)$. These singularities can be resolved by cutting out the cones and gluing in the disk bundles over S^2 of Euler class -6, -3, and -2 respectively. The torus fiber is homologous to $6X + A + 2B + 3C$, and setting its square equal to zero and solving gives $X \cdot X = -1$. This gives the first picture in Figure 3.6, which is followed by a sequence of blowdowns to produce the neighborhood $N(\text{II})$ of the cusp.
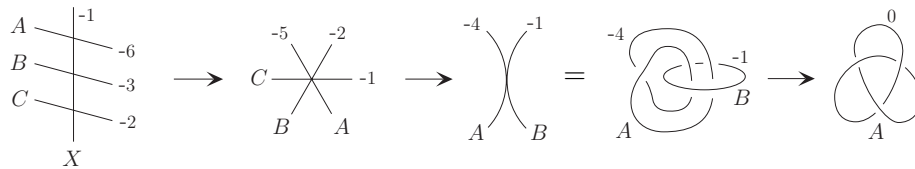

Figure 3.6: Blowing down to $N(\text{II})$

In the compactness theorem, the torus fiber bubbles off a 2–sphere at each of the six branch points a, b, b', c, c', c''. The torus then 6–fold covers X while bubble a hits A, the two bubbles b, b' hit B, and the three bubbles c, c', c'' hit C. Finally this map is composed with the sequence of three blowdowns to give a degeneration to the cusp. Since the blowdowns burst all but the first bubble, this amounts to one bubble which maps onto the cusp while the torus is mapped (by the constant holomorphic map) to the singular point of the cusp (Figure 3.7).

Type II* We use the same construction for E as in the previous case for II, but the orientation is changed. This is because the rational elliptic surface $E(1)$ equals II and II* glued along their common boundary. So E is now desingularized by removing the cones on $L(6, 5)$, $L(3, 2)$, and $L(2, 1)$ and replacing them
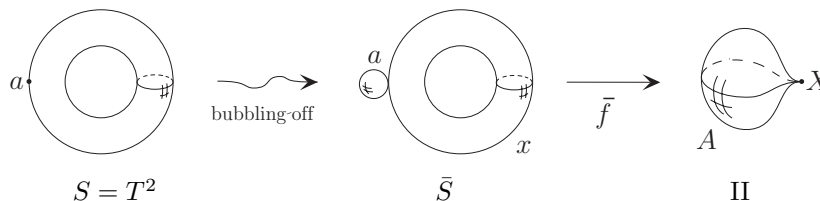
Figure 3.7: Degeneration to II

by linear plumbings (of disk bundles of Euler class -2) of length 5, 2 and 1 respectively (Figure 3.8). This is $N(\text{II}^*)$; note that $X \cdot X = -2$ by the usual calculation.
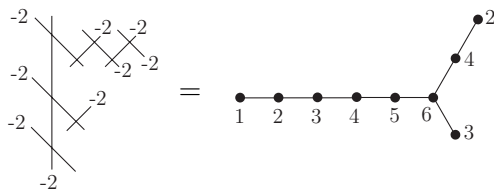

Figure 3.8: $N(\text{II}^*)$

For the compactness theorem, the torus bubbles off a linear graph of five bubbles at the fixed point a, a line of two bubbles at each of the two points b, b' with stabilizer $\mathbb{Z}_3$, and one bubble at each of the three points c, c', c'' with stabilizer $\mathbb{Z}_2$ (see Figure 3.9). Then the torus 6–fold covers X; each of the five bubbles in the linear graph 5–fold cover (with two branch points), 4–fold cover, 3–fold cover, 2–fold cover (still with two branch points where they intersect their neighbors), and 1–fold cover, the long arm of II*; the pair of two bubbles each will 2–fold cover and 1–fold cover, providing multiplicities 4 and 2 since there are two pairs; the three single bubbles all map onto the short arm of II* giving multiplicity 3. Note that the labels for the bubbles have been chosen so that bubble a_i maps to A_i by an i–fold branched covering, and similarly for the b and c–bubbles.

We can now abbreviate the description for III and IV and their duals for the arguments are similar to II and II* with no new techniques.

Type III Again consider the torus as the square with opposite sides identified and let σ_4 be rotation by $\pi/2$. This has fixed points at the center of the square and at the vertex, and an orbit of two points equal to the midpoints of the sides with stabilizer $\mathbb{Z}_2$. We resolve the quotient $T^2 \times B^2/\sigma_4 \times \tau_4$ by cutting
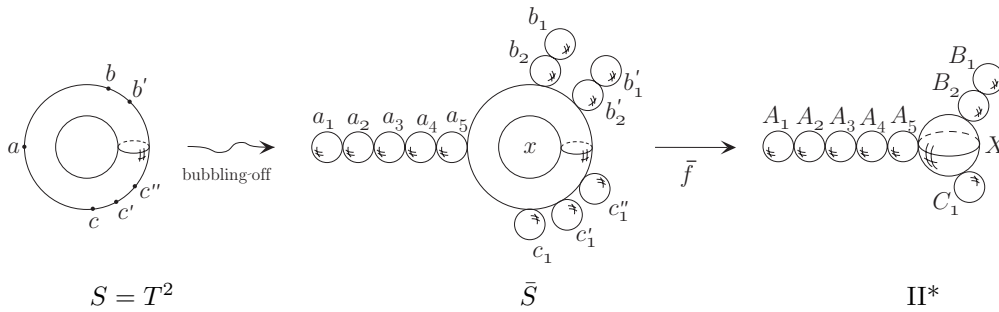
Figure 3.9: Degeneration to II*

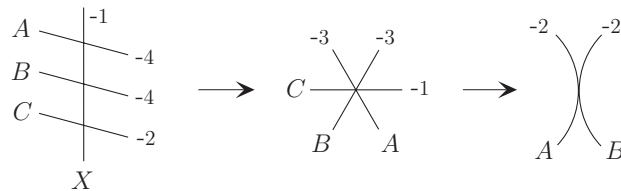out cones and gluing in disk bundles, and a sequence of blowdowns gives the neighborhood $N(\mathrm{III})$ shown in Figure 3.10.

Figure 3.10: Blowing down to $N(\mathrm{III})$

Now, as in II, the torus bubbles off 2–spheres which map and then in some cases blow down, to give a composition in which two bubbles survive and map onto the two curves in III and the torus maps to the point of tangency (Figure 3.11).
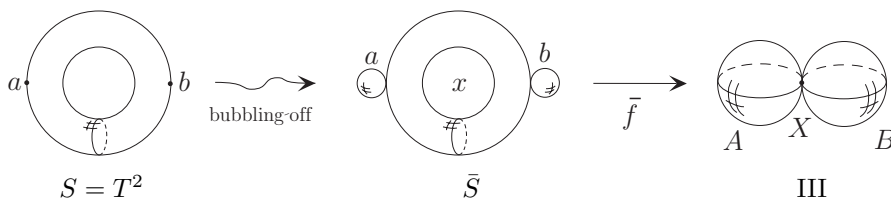

Figure 3.11: Degeneration to III

Type III* As with II*, we reverse orientation, cut out the cones and replace them with linear plumbings to get $N(\mathrm{III}^*)$ (Figure 3.12).

We then get a degeneration of the torus fiber very similar to II*, using the torus as a 4–fold branched cover of S^2 with three branch points of indices 4, 4, and 2 (Figure 3.13).
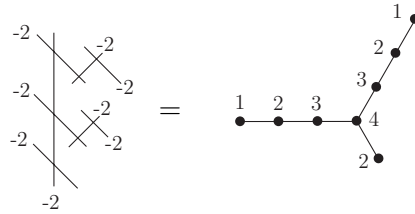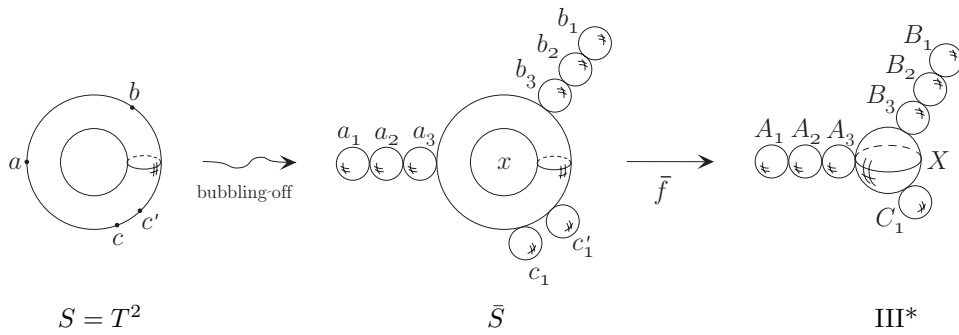
Figure 3.12: $N(\text{III*})$

$S = T^2$ $\bar{S}$ III*

Figure 3.13: Degeneration to III*

Type IV   Here we define a $\mathbb{Z}_3$ action on the torus by simply squaring the action given in II. The center and any two adjacent vertices of the hexagon represent the three fixed points a, b and c ($= b'$ in Figure 3.2b). Proceeding as before, we get the singular fiber drawn in Figure 3.14. Blowing down once gives $N(\text{IV})$.
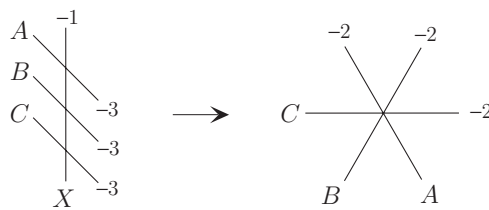

Figure 3.14: Blowing down to $N(\text{IV})$

The torus now bubbles off three 2–spheres which hit the three curves in IV while the torus maps to the triple point (Figure 3.15).

Type IV*   Arguments similar to those above give $N(\text{IV*})$ (Figure 3.16) as well as the degeneration of the torus fiber (Figure 3.17).
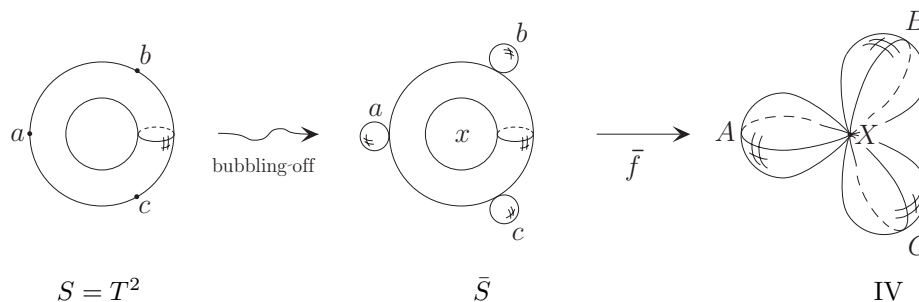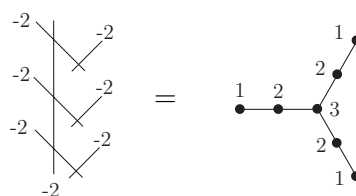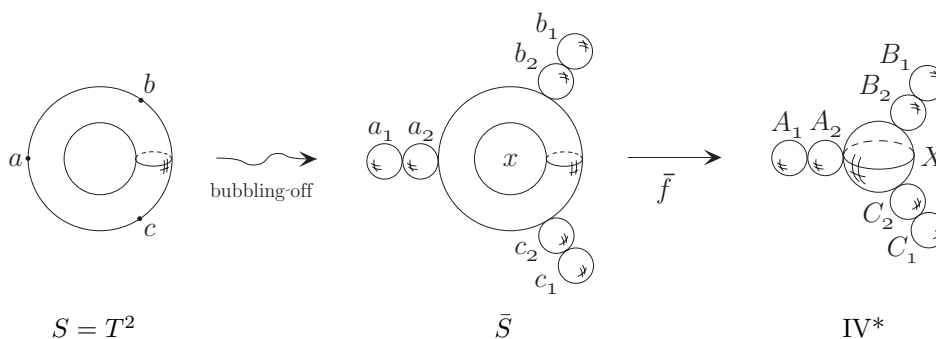
Figure 3.15: Degeneration to IV

Figure 3.16: $N(\text{IV}^*)$

Figure 3.17: Degeneration to IV*

References

[1] **S Akbulut**, **R C Kirby**, *Branched covers of surfaces in 4–manifolds*, Math. Ann. 252 (1980) 111–131

[2] **E Brieskorn**, *Uber die Auflösung gewisser Singularitäten von holomorphen Abbildungen*, Math. Ann. 166 (1966) 76–102

[3] **E Brieskorn**, *Die Auflösung der rationalen Singularitäten holomorphen Abbildungen*, Math. Ann. 178 (1968) 255–270

[4] **E Brieskorn**, *Singular elements of semi-simple algebraic groups*, Proc. I.C.M., Nice (1970) 279–284

[5] **R E Gompf**, **A I Stipsicz**, *4–Manifolds and Kirby Calculus*, Grad. Studies in Math. 20, Amer. Math. Soc. (1999)

[6] **M Gromov**, *Pseudo holomorphic curves in symplectic manifolds*, Invent. Math. 82 (1985) 307–347

[7] **J L Harer**, **A Kas**, **R C Kirby**, *Handlebody decompositions of complex surfaces*, Memoirs AMS 62, number 350 (1986)

[8] **C Hummel**, *Gromov's Compactness Theorem for Pseudo-holomorphic Curves*, Progress in Math. 151 Birkhaüser (1997)

[9] **A Kas**, *On the handlebody decomposition associated to a Lefschetz fibration*, Pac. J. Math. 89 (1980) 89–104

[10] **R C Kirby**, *A calculus for framed links in S^3*, Invent. Math. 45 (1978) 36–55

[11] **R C Kirby**, **M G Scharlemann**, *Eight faces of the Poincaré homology 3–sphere*, from: "Geometric Topology", Proc. 1977 Georgia Topology Conf. (J C Cantrell, editor) Academic Press (1979) 113–146

[12] **K Kodaira**, *On compact analytic surfaces III*, Ann. Math. 78 (1963) 563–626

[13] **Little Richard**, *Slippin' an' a Slidin'*, Motown (1956)

[14] **T H Parker**, **J G Wolfson**, *Pseudoholomorphic maps and bubble trees*, J. Geom. Anal. 3 (1993) 63–98

University of California, Berkeley, CA 94720, USA
Bryn Mawr College, Bryn Mawr, PA 19010, USA

Email: `kirby@math.berkeley.edu`, `pmelvin@brynmawr.edu`